



RESEARCH ARTICLE

10.1029/2018JC014479

Green Icebergs Revisited

Stephen G. Warren¹ , Collin S. Roesler², Richard E. Brandt³, and Mark Curran⁴

Key Points:

- Icebergs of marine ice vary in color from blue to green
- The color is probably caused more by iron oxides than by dissolved organic carbon
- The color may indicate the ability of icebergs to deliver iron as a nutrient

Correspondence to:

S. G. Warren,
sgw@uw.edu

Citation:

Warren, S. G., Roesler, C. S., Brandt, R. E., & Curran, M. (2019). Green icebergs revisited. *Journal of Geophysical Research: Oceans*, 124. <https://doi.org/10.1029/2018JC014479>

Received 14 AUG 2018

Accepted 6 JAN 2019

Accepted article online 10 JAN 2019

¹Department of Atmospheric Sciences, University of Washington, Seattle, WA, USA, ²Department of Earth and Oceanographic Science, Bowdoin College, Brunswick, ME, USA, ³Atmospheric Sciences Research Center, University at Albany - State University of New York, Wilmington, NY, USA, ⁴Australian Antarctic Division, Kingston, Tasmania, Australia

Abstract Ice crystals form in supercooled seawater beneath several Antarctic ice shelves; as they rise to the ice-shelf base they scavenge particles from the water and incorporate them into the growing basal ice. The resulting *marine ice* can be ~100 m thick; it differs from sea ice in that it is clear, desalinated, and bubble-free. Icebergs of marine ice vary in color from blue to green, depending on the nature and abundance of foreign constituents in the seawater that became trapped in the ice as it grew. A red or yellow material (i.e., one that absorbs blue light), in combination with the blue of ice, can shift the wavelength of minimum absorption to green. Previously, dissolved organic carbon (DOC) had been proposed to be responsible for the green color. Subsequent measurements of low DOC values in green icebergs, together with the recent finding of large concentrations of iron in marine ice from the Amery Ice Shelf, suggest that the color of green icebergs is caused more by iron-oxide minerals than by DOC. These icebergs travel great distances from their origin; when they melt they can deliver iron as a nutrient to the Southern Ocean.

Plain Language Summary Glacier ice, originating from snowfall, flows off the Antarctic Ice Sheet to float on the ocean as ice shelves. At the front of the ice-shelf, icebergs break off. They appear bluish-white, intermediate between the blue of pure ice, and the white of snow, because glacier ice contains numerous bubbles that scatter light. Seawater freezes to the base of some ice shelves, forming *marine ice*, which incorporates organic and inorganic particles from the water. On the resulting composite icebergs, the marine ice can be exposed to view if the iceberg capsizes. The marine-ice part of such icebergs is clear, dark, and often green in color, because red or yellow particles from the seawater, in combination with the blue of ice, can shift the color to green. Previously, dissolved organic carbon had been proposed to be responsible for the green color. The recent finding of large concentrations of iron in marine ice from the Amery Ice Shelf suggests that the color of green icebergs is caused more by iron-oxide minerals. These icebergs travel great distances from their origin; when they melt they can deliver iron as a nutrient to the Southern Ocean.

1. Introduction

1.1. Glaciers, Ice Shelves, and Icebergs

Glacier ice is formed by compression of snow under its own weight. The air in the snow becomes closed off as the snow grains coalesce, so glacier ice contains numerous bubbles. The Antarctic Ice Sheet flows outward to the coast, where the climate is warmer than in the interior but still too cold to allow much surface-melting, so the ice flows out to float on the ocean as an ice shelf, typically several hundred meters thick. Where the ice sheet loses its contact with the bedrock and begins floating is called the grounding line. At the front of the ice shelf, where tides, swell, and currents cause cracks to form, icebergs break off (calve) and float away. The icebergs consist partly of snow and partly of bubbly glacier ice, so they have high albedo and appear white like snow or bluish-white, intermediate between the white of snow and the blue of pure ice. Pure ice is blue because its absorption coefficient in the visible range increases with wavelength from blue to red; the absorption length (i.e., the mean free path of a photon before absorption) is ~2 m for red light but ~200 m for blue light (Warren & Brandt, 2008). The addition of bubbles causes the photons to change direction repeatedly by refraction, reemerging at the surface after passing only a short distance through ice ($\ll 2$ m), which leads to a whitening of the blue color.

1.2. Marine Ice Versus Sea Ice

At the base of an ice shelf, both melting and freezing can occur along the ice/ocean interface, with melting dominating on average. Where freezing does occur, the frozen seawater can build up a thick layer at the base

©2019. The Authors.

This is an open access article under the terms of the Creative Commons Attribution-NonCommercial-NoDerivs License, which permits use and distribution in any medium, provided the original work is properly cited, the use is non-commercial and no modifications or adaptations are made.

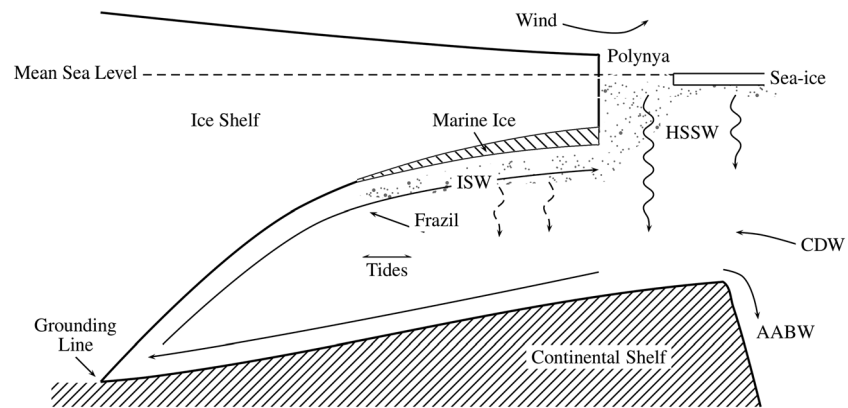


Figure 1. Schematic vertical cross section of an Antarctic ice shelf and its environment, particularly applicable to the Amery Ice Shelf. (reproduction of Figure 2 of Galton-Fenzi et al., 2012). Water-mass abbreviations are for ice-shelf water (ISW), high-salinity shelf water (HSSW), circumpolar deep water (CDW), and Antarctic bottom water (AABW).

of the ice shelf, in places comprising as much as one third of the ice-shelf thickness (Morgan, 1972). This basal ice is given the name *marine ice* to distinguish it from sea ice, because its freezing conditions and structure are different.

Sea ice is formed by freezing of seawater at the ocean surface, with typical thickness ~1 m. It contains both brine inclusions and air bubbles. As seawater freezes, salt ions are excluded from the ice lattice structure. However, depending upon the rate of freezing, not all of the salt is left behind in the ocean. About 30% of the salt is trapped in pockets within the ice, resulting in bulk salinity of ~10‰ by mass in newly formed sea ice (Kovacs, 1996; Wadhams, 2000).

Several processes can be responsible for the presence of bubbles in sea ice (Tsurikov, 1979). Most bubbles are located within brine inclusions (Light et al., 2003), suggesting that the most important mechanism is the following: As water in a brine inclusion freezes, shrinking the volume of liquid, the remaining brine becomes supersaturated with air, leading to formation of a bubble within the brine inclusion (Moreau et al., 2014).

Marine ice, by contrast, forms at higher pressure at ~400-m depth, where air is more soluble than at the ocean surface, so the water is undersaturated and the air that would be rejected in the freezing process can remain dissolved in the water below the ice, rather than forming bubbles that could be trapped in the ice. Marine ice is also effectively desalinated, with salinity typically 2 to 3 orders of magnitude smaller than that of seawater, but the remaining salts still have ionic ratios that are the same as in seawater (Table 1 of Warren et al., 1993). The mechanism for this extreme desalination is not completely understood (Tabraham, 1997; section 4.4 of Eicken et al., 1994).

The actual mechanism of freezing is important for explaining the colors of marine ice. Figure 1, from Galton-Fenzi et al. (2012), is a schematic vertical cross section of an ice shelf, particularly applicable to the Amery Ice Shelf, the largest ice shelf in East Antarctica (Figure 2). There is an inflow of circumpolar deep water (CDW) over the continental shelf. At the grounding line at 2,400-m depth, the CDW melts enough ice to lower the water temperature to the local freezing point, which is -3.7°C , determined by the combination of salinity and pressure. The cold water, now called ice-shelf water, is buoyant because of its reduced salinity after entrainment of some glacial meltwater. The ice-shelf water flows up under the ice ceiling to lower pressure, where it finds itself supercooled because of the pressure dependence of melting temperature.

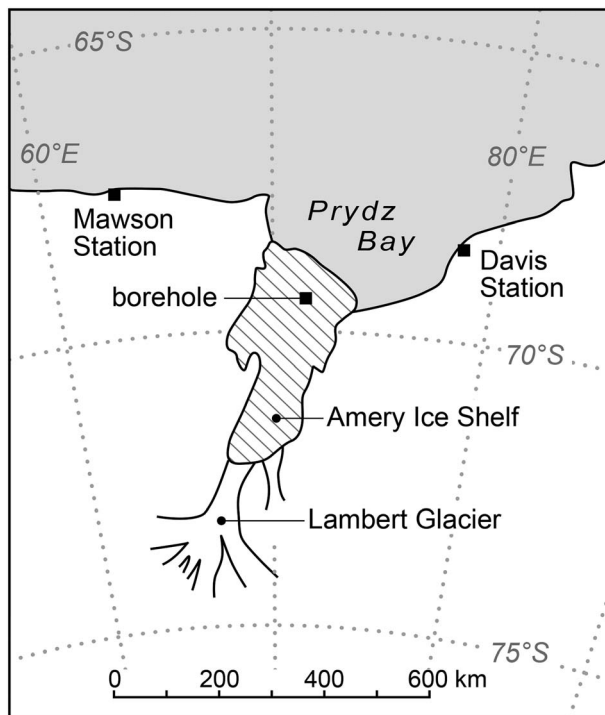


Figure 2. The Amery Ice Shelf and its surroundings. Icebergs of marine ice were sampled near Mawson Station and Davis Station.

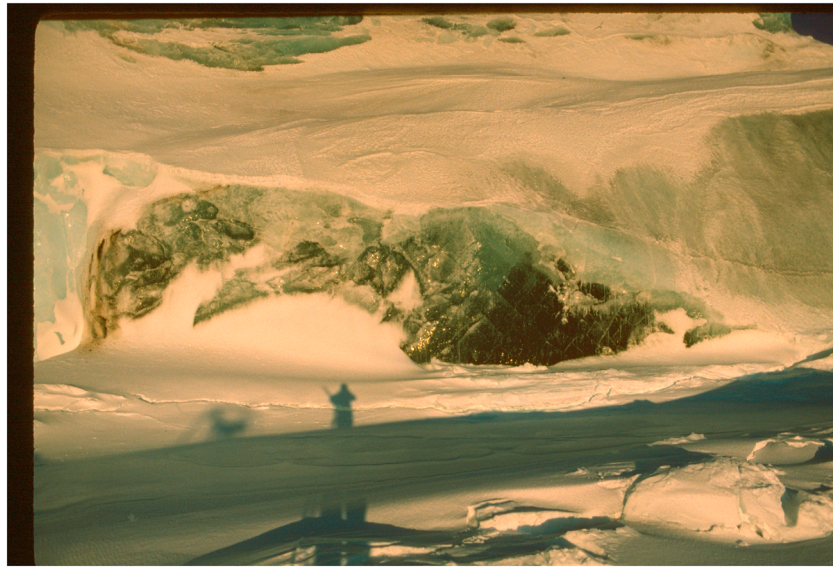


Figure 3. Close-up view of an iceberg near Mawson Station, 20 November 1988, much of it covered by snow. At the far left is bubbly blue-white glacier ice; the center of the picture shows the clear, dark green, bubble-free marine ice. The boundary between glacier ice and marine ice is nearly vertical.

The supercooled water requires nucleation sites to form ice crystals (*frazil ice*). These nucleation sites may be organic or inorganic particles suspended in the water column. The frazil crystals are less dense than water, so the crystals with their nuclei float up to accrete to the ice-shelf base. As they rise, they can scavenge other organic and inorganic particles or large molecules from the water and incorporate them into the basal ice. In particular, small mineral particles of *glacier flour* are produced by erosion of bedrock at the base of the ice sheet; many of these particles are small enough to have a long lifetime suspended in the seawater below the ice shelf.

The Amery is particularly suitable for formation of marine ice because its grounding line is so deep (Silvano et al., 2016). The inflow of CDW occurs on the eastern side of the ice shelf, and the marine ice forms mostly on the western side (Fricker et al., 2001). If the marine ice does not melt off the bottom before reaching the calving front, the icebergs calving into Prydz Bay will contain two types of ice: the upper part glacier ice and the lower part marine ice. This marine ice is hidden below the water-line, but if the horizontal extent of the iceberg is small enough, it may capsize, exposing the marine ice.

1.3. Green Icebergs

The color of marine ice is affected by the composition and concentration of the foreign materials that were incorporated into the basal ice as it grew. In the literature of the last century there were occasional reports of green icebergs (Amos, 1978; Dieckmann et al., 1987; Drygalski, 1921; Moulton & Cameron, 1976; Reichelt, 1941; Wordie & Kemp, 1933). In some icebergs the ice was so dark that it appeared black (Binder, 1972). At close range, what is most distinctive about the appearance of these icebergs is not their color but rather their clarity. Because they lack bubbles, these icebergs are clear and quite dark (Figure 3). The connection between the literature on green icebergs and the literature on basal freezing to ice shelves was made by Kipfstuhl et al. (1992), confirmed by Warren et al. (1993). *Jade bergs* are commonly seen by residents of Davis and Mawson stations on opposite sides of Prydz Bay (Figure 2), and this is the region where we have had the opportunity to sample them.

1.4. Striped Icebergs

Icebergs consisting mainly of glacier ice may contain parallel stripes of marine ice, as shown in Figure 4. These stripes probably result from tension at the ice-shelf base generating basal crevasses (Dutrieux et al., 2014) that immediately flood with seawater, which quickly freezes. Samples taken every few centimeters across one of these stripes gave the oxygen-isotope profile shown in Figure 5, which confirms that the stripe consists of marine ice surrounded by glacier ice. Glacial ice originates from snowfall, so it is isotopically light.



Figure 4. Stripes of marine ice within an iceberg of glacier ice, most likely formed by seawater filling bottom-crevasses formed as tension-cracks (30 October 1996, north of Davis Station).

Values of $\delta^{18}\text{O}$ in the Amery Ice Shelf range from -20 to -40‰ (Morgan, 1972), in comparison to $\delta^{18}\text{O} \approx 0$ for seawater and $\delta^{18}\text{O} \approx +2\text{‰}$ for marine ice. Figure 5 was drawn to emphasize the small variations within the marine ice, so it does not extend down to show the value for the surrounding glacial ice, which had $\delta^{18}\text{O} \approx -20\text{‰}$. The approximate left-right symmetry of $\delta^{18}\text{O}$ is consistent with the freezing having proceeded symmetrically from the opposite walls of the crevasse.

Striped icebergs were apparently first reported by Reichelt (1941, page 13). Khazendar et al. (2001) were able to obtain a core through the full length of a marine-ice stripe on the Nansen Ice Shelf by the Ross Sea, where marine ice outcrops because of intense sublimation at the surface. That stripe was much wider than the ones we have seen.

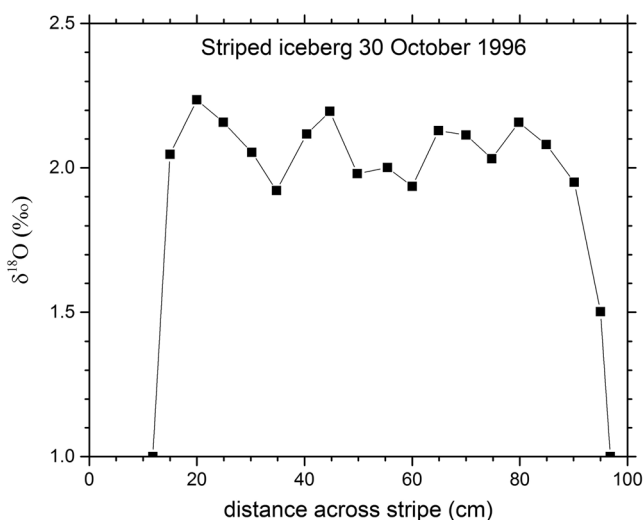


Figure 5. Oxygen isotopes measured across a stripe of marine ice within glacier ice (photo in Figure 4). At the left and right ends of the plot, $\delta^{18}\text{O}$ descends to the negative values of the glacier ice, $\sim -20\text{‰}$, far below the range of this plot. Here we have expanded the region of the marine ice to show the small variations that exhibit approximate mirror-symmetry.

2. Marine Ice: Blue or Green?

Our 1993 paper concerned measurements on an iceberg that we had sampled in 1988 near Mawson Station while on a sea ice expedition; that iceberg was green (Figure 3). Our next opportunity to sample marine ice was on another sea ice expedition in 1996 (Warren et al., 1997), where we became aware that not all marine ice is green. On the iceberg shown in Figure 6, the boundary between glacier ice and marine ice (originally horizontal) is near the left end of the photo, tilted $\sim 60^\circ$. This marine ice has the color expected for nearly-pure ice. The ice contains cracks, spaced ~ 1 m apart, probably caused by release of pressure or exposure to the cold air as the iceberg turned onto its side. These cracks provide the only opportunities for sunlight to be refracted and returned to the viewer. Because of the long pathlengths between scattering events, the longer wavelengths of visible light are absorbed, and only blue survives.

The marine ice in this iceberg was not uniform in composition. It contained a large volume of blue ice, shown in Figure 6, but some parts of this iceberg were green or yellow-green. We measured spectral albedos of all these surfaces, as well as the glacier ice. Figure 7 shows that the albedo of the glacier ice exceeds that of the marine ice at all wavelengths. The albedo of blue marine ice peaks at ~ 470 nm, the green marine ice at ~ 540 nm, and yellow-green marine ice at 570 nm. Since the wavelength of minimum absorption for pure ice is in the ultraviolet (UV) at

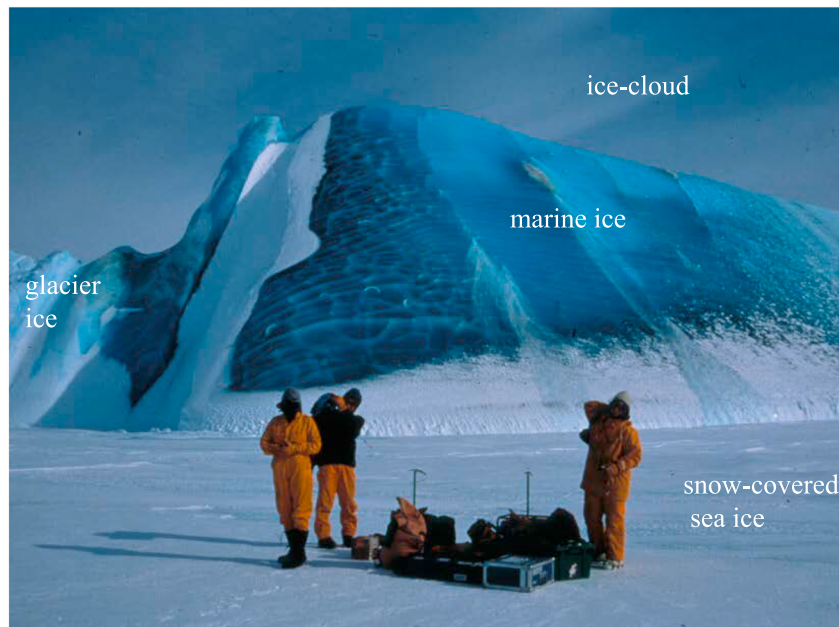


Figure 6. Iceberg at 68.25°S, 78.27°E, 36 km north of Davis Station, on 31 October 1996. There are five kinds of ice in this picture: sea ice, snow, glacier ice, marine ice, and ice cloud. [Photo by Stephen Warren. A version of this photograph was previously published in *Science Advances* by Hoffman et al. (2017).]

$\lambda < 390$ nm (Figure 8), even the blue marine ice must contain some non-ice constituents that have shifted the peak albedo from UV to blue. We also measured the spectral absorption of the meltwater from each of these ice surfaces; the results are consistent with the differences in their albedo spectra.

3. Can Organic Carbon Explain the Colors?

3.1. The Green Iceberg From 1988

The absorption coefficient of ice increases with wavelength from blue to red (Figure 8, lower curve). Adding a blue-absorbing constituent can shift the absorption-minimum to longer wavelength, toward green. Our

hypothesis for the 1988 green iceberg near Mawson Station was that the green color was caused by colored dissolved organic matter (CDOM), which is known to be responsible for the green or yellow colors of seawater in coastal waters near river systems (Morel & Prieur, 1977). Fluorescence of meltwater samples from the iceberg confirmed the presence of CDOM and suggested that the ice contained dissolved organic carbon (DOC), but at that time we did not have the means to quantify the DOC. We nevertheless proposed DOC as the explanation for the green color (Warren et al., 1993).

3.2. DOC in the Multicolored Iceberg From 1996

The different parts of this iceberg were measured for oxygen isotopes, DOC, and ions. The ions were present in near-seawater ratios; in the marine ice the bulk salinity was $\sim 0.1\%$; that is, about 1/300 that of seawater (Table 1). Salinity (S) was estimated from the measured chloride concentration using the conversion $S (\%) = [\text{Cl}^-] (\text{mg/L}) \times 0.0018066$. Chloride concentrations were measured using ion chromatography, similar to the method of Curran and Palmer (2001).

The oxygen isotopes and DOC are also given in Table 1. DOC was measured on acidified samples by high-temperature combustion and subsequent quantification of the CO_2 gas (Peltzer & Hayward, 1996; Vlahos

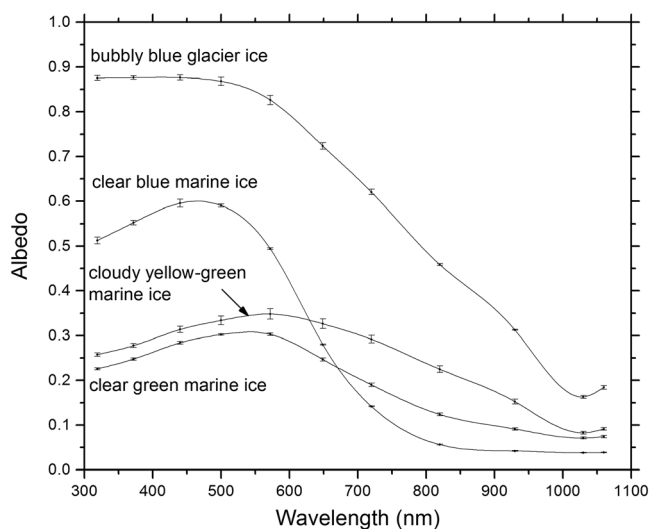


Figure 7. Spectral albedos of different locations on the iceberg shown in Figure 6. Oxygen-isotope analyses (Table 1) identify the bubbly blue ice as glacial ice formed by compression of snow; the other ice types were formed by freezing of seawater. The curves are spline-fits to the data points.

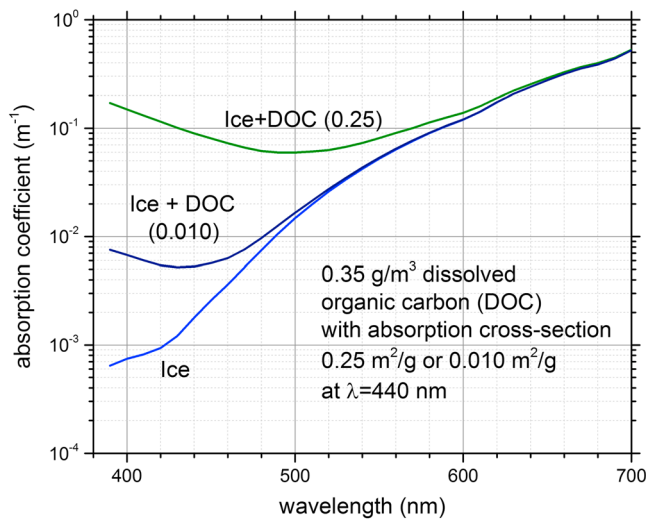


Figure 8. Sum of absorption coefficients of dissolved organic carbon (DOC) and ice versus wavelength. The DOC spectrum was taken from Figure 1b of Yacobi et al. (2003). Two illustrative values are taken for the mass-absorption cross-section B_a at $\lambda = 440$ nm: $0.25 \text{ m}^2/\text{g}$ (from Yacobi et al. for rivers entering the Gulf of Mexico on the Georgia-Florida border) and $0.010 \text{ m}^2/\text{g}$ (from Figure 9; sea ice at the Arctic coast of Alaska). The spectrum of ice is from Warren and Brandt (2008).

et al., 2002). The DOC values in the blue-marine, green-marine, and glacial ice are all similar, 0.3–0.5 mg/L; that of the yellow-green ice is higher. The DOC values correlate with salinity, suggesting that the desalination process also affects the entrainment of DOC. Except for the yellow-green ice, these DOC values are slightly lower than those found in deep water of the Antarctic Circumpolar Current and the Ross Sea, 0.5 mg/L (Hansell & Carlson, 1998), and in surface waters at 60°S , 0.6 mg/L (Ogawa et al., 1999). A green iceberg sampled in 1994 near Mawson Station (also listed in Table 1) had similar DOC = 0.35 mg/L. The similarity of the DOC values for blue and green ice already casts doubt on DOC as being responsible for discriminating the colors. Nevertheless, before seeking an alternative explanation for the color, we will compute the possible contribution of DOC.

4. Absorption Spectra of Dissolved Organic Matter

“Dissolved” organic matter (DOM) is mostly not dissolved at the molecular level. Instead, the “dissolved” fraction means the fraction that passed through a specified filter, typically meaning particle diameters <0.45 or $<0.2 \mu\text{m}$. Much of the DOM does not significantly absorb visible light. The fraction that does absorb is called chromophoric (or colored) DOM (CDOM) (Nelson & Siegel, 2013). Most CDOM in the ocean has a terrestrial source, so the concentrations of CDOM are high in river estuaries and decrease with distance from the coast into the open ocean. In a sam-

ple of DOM, the CDOM can increase with bacterial decomposition, and it can decrease by exposure to sunlight (bleaching). The global map in Figure 4 of Nelson and Siegel (2013) shows values in Prydz Bay (in front of the Amery Ice Shelf) about 10 times higher than in the remote Southern Ocean.

In fact, the *O* in the acronym CDOM, meaning *organic*, is misleading. CDOM is usually quantified by the spectral absorption of the water, or remotely sensed color, so the color attributed to organic matter could instead be caused by inorganic blue-absorbers. In our paper proposing DOC as the explanation of the green

Table 1
Oxygen Isotopes, Salinities, and Dissolved Organic Carbon (DOC) in Icebergs and Basal Ice

Location	Date sampled	Sampled by	Ice type, color	$\delta^{18}\text{O}$ (‰)	Salinity (‰)	DOC (mg/L = g/m ³)	DOC analyzed by
Icebergs, 36 km north of Davis Station. 68°S , 78°E	31 October 1996	Roesler et al.	bubbly-blue (glacial)	-17.7	0.11	0.46	Robert Chen (Univ. Mass.) 1998
			green (marine)	2.2	0.11	0.42	
			blue (marine)	2.3	0.08	0.35	
			yellow-green (marine)	1.9	0.14	1.30	
Icebergs near Mawson Station 68°S , 63°E	1994	Mawson personnel	green, clear (several icebergs)			0.35	John Gibson (at Davis), 1995
Iceberg, Cap Norvegia. 72°S , 18°W	16 February 1985	Dieckmann	green (Kipfstuhl et al., 1992)	1.6 to 2.5		0.18, 1.05, 0.11	Roesler Kipfstuhl
Basal ice from Filchner-Ronne Ice Shelf	1990	Kipfstuhl (Oerter et al., 1992)		1.7 to 2.6		0.6 to 3.4, 0.26	Roesler Kipfstuhl
Iceberg near Mawson. 67°S , 62°E	19 November 1988	Brandt and Warren	green (Warren et al., 1993, Table 1)	2	0.03		
Iceberg near Mawson. 67°S , 63°E	1986	Allison	green (Warren et al., 1993, Table 1)		0.16		

Note. Salinities (*S*) were estimated from measured chloride concentrations using the conversion $S (\text{‰}) = [\text{Cl}^-] (\text{mg/L}) \times 0.0018066$. The measurement uncertainty for DOC is ± 0.05 mg/L.

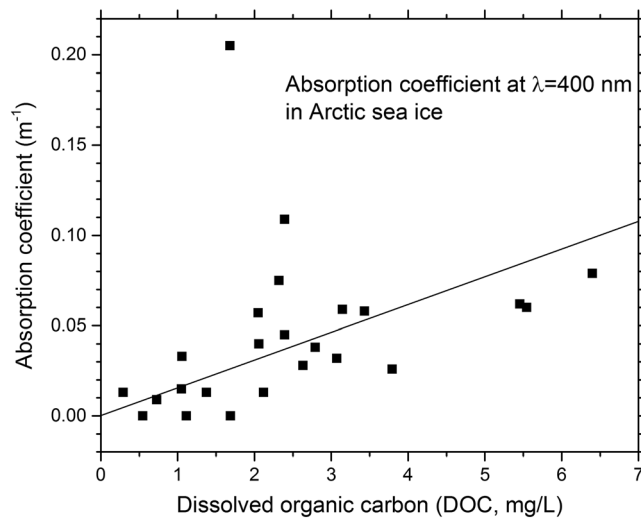


Figure 9. Absorption coefficient (at $\lambda = 400$ nm) versus dissolved organic carbon (DOC), for sea ice near Utqiagvik (Barrow), Alaska, in April 1995. The least squares line gives a mass absorption cross section (*mass-specific absorption*) $B_a = 0.0154$ m²/g at $\lambda = 400$ nm, with correlation $r^2 = 0.50$. Using the spectral slope of Yacobi et al. (2003), this corresponds to $B_a = 0.010$ m²/g at $\lambda = 440$ nm.

absorption likewise decreases strongly with wavelength from UV to red. Figure 1 of Russell et al. (2010) shows that a power-law relation provides an excellent fit to many aerosol spectra: $k_a = b\lambda^{-t}$, with $t \approx 5$ for organic-carbon aerosols (humic-like materials). The exponent t is called the Ångström exponent. Apparently neither an exponential dependence nor a power law dependence has any theoretical justification; they are both just convenient empirical ways to describe measurements. Twardowski et al. (2004) showed that power-law fits are better than exponential fits for CDOM in seawater, but the exponential description remains the most popular in the oceanographic literature.

In summary, the description of absorption spectra for DOC requires a value of s (or t) for the spectral shape and a value of k_a at a specified wavelength to anchor the function. Yacobi et al. (2003) measured absorption spectra of water in rivers in the Georgia-Florida border region. They also measured DOC in the water, segregated by molecular size. Dividing k_a by their measured DOC concentrations gave values of B_a that varied with molecular size, from 0.08 to 1.9 m²/g at $\lambda = 440$ nm, but bulk samples were all near 0.25 m²/g. Their spectral slope was $s \approx 0.015/\text{nm}$, in agreement with Bricaud et al. (1981). Alternatively, we can get a very good fit to their plot using a power law dependence, with $t \approx 5$.

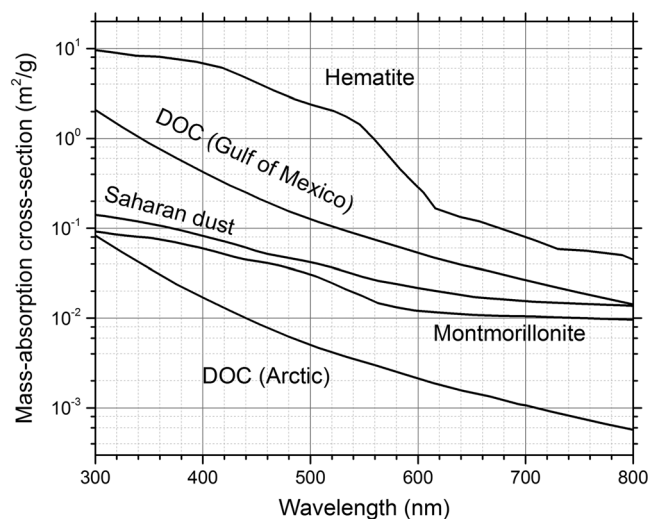


Figure 10. Mass absorption cross section B_a for hematite (Glasscock et al., 2008), atmospheric mineral dust typical of the Sahara (Dang et al., 2015), montmorillonite, and two types of dissolved organic carbon (DOC; see caption of Figure 8 for sources).

color of a jade berg, we compared the absorption spectrum of the iceberg meltwater to that of seawater in Prydz Bay, 50 km out from the front of the Amery Ice Shelf (Figure 4 of Warren et al., 1993). The minimum of the seawater absorption coefficient was at 570 nm, indicating the presence of blue-absorbing constituents, which we thought would be DOC, but they could instead have been iron minerals, or a combination of DOC and iron, as neither DOC nor iron were measured.

Because CDOM is a variable fraction of DOM, the mass-absorption cross-section B_a (units m²/g, often called *mass-specific absorption*) reported for DOC at a particular wavelength (typically 412 or 440 nm) varies widely. We need B_a to convert a concentration of DOC (g/m³) to a linear absorption coefficient k_a (m⁻¹). Hansen et al. (2016) reported values ranging from 0.02 to 0.65 m²/g, depending on biodegradation and photoexposure. Fichot and Benner (2011) reported values in the Gulf of Mexico, off Louisiana, ranging from 0.04 m²/g for oligotrophic water to 2.2 m²/g for fresh water.

The absorption coefficients of DOC (k_a , units m⁻¹) are always found to decrease strongly with wavelength from UV to red. By convention, they are fit to an exponential function, $k_a = ce^{-s\lambda}$, with s typically about 0.015/nm (Bricaud et al., 1981). The use of an exponential fit, apparently first introduced by Jerlov (1968), is in contrast to the convention used to represent absorption spectra of atmospheric aerosols, whose absorption likewise decreases strongly with wavelength from UV to red. Figure 1 of Russell et al. (2010) shows that a power-law relation provides an excellent fit to many aerosol spectra: $k_a = b\lambda^{-t}$, with $t \approx 5$ for organic-carbon aerosols (humic-like materials). The exponent t is called the Ångström exponent. Apparently neither an exponential dependence nor a power law dependence has any theoretical justification; they are both just convenient empirical ways to describe measurements. Twardowski et al. (2004) showed that power-law fits are better than exponential fits for CDOM in seawater, but the exponential description remains the most popular in the oceanographic literature.

The measurements for rivers in Georgia and Florida may not be applicable to polar oceans. We therefore also make use of absorption measurements (Perovich et al., 1993; Roesler & Iturriaga, 1994) and associated DOC measurements (unpublished) in sea ice on the north coast of Alaska. The absorption coefficient k_a (at 400 nm) exhibits a strong relationship with DOC (Figure 9); the least squares line indicates $B_a = 0.0154$ m²/g. Using the spectral dependence from Yacobi et al. (2003) to adjust from 400 to 440 nm, this corresponds to $B_a = 0.010$ m²/g at $\lambda = 440$ nm, that is, a factor of 25 smaller than the Florida values.

5. Combining Absorption Spectra of DOC and Ice

We accept the spectral slope from Yacobi et al. (2003), then apply either the Florida or the Alaska values of B_a . The resulting spectra $B_a(\lambda)$ are

shown in Figure 10. The absorption coefficient of DOC (units m^{-1}) is then $k_a = B_a \times [\text{DOC}]$, where we use $[\text{DOC}] = 0.35 \text{ mg/L}$ (equivalent to g/m^3) from Table 1. Figure 8 shows that using the Florida B_a , this amount of DOC would shift the wavelength of minimum absorption (λ_{min}) to 500 nm (green), but the Alaskan value of B_a would keep it in the blue ($\lambda_{\text{min}} = 430 \text{ nm}$).

It seems likely that the Alaskan sea ice value of B_a , as representing a polar ocean, would be the more appropriate choice for DOC in water under the Amery Ice Shelf. If so, the DOC concentration measured in the 1996 icebergs is sufficient to shift the peak albedo from 390 nm (UV) to 430 nm (blue), but insufficient to cause a green color. To acquire a green color, the ice would have to contain 9 g/m^3 of DOC, that is, 25 times the observed value.

Table 1 offers yet another puzzle, in that the glacial ice also contains DOC at amounts similar to the marine ice. This DOC may have been acquired by infiltration of seawater during an earlier capsizing event, as this glacial ice also contains salts in seawater ratios, with total salinity $\sim 0.1\%$. In any case, the DOC values in Table 1 for the blue-marine and green-marine ice are the same, within experimental uncertainty. The lack of distinctive differences in DOC concentration between blue ice and green ice motivates us to consider an alternative explanation for their different colors.

6. Iron in Marine Ice

The recent finding of large concentrations of iron in marine ice offers an attractive explanation for the color of green icebergs, and perhaps even the opportunity to use color as an assay for the iron content. Herraiz-Borreguero et al. (2016; hereafter HB) used the Amery core that had been drilled in 1968 (Morgan, 1972) at the borehole location shown in Figure 2. HB took samples of ice from above and below the glacial/marine transition and analyzed them for iron. Filtration of the meltwater separated the iron into two fractions: water that passed through a $0.2\text{-}\mu\text{m}$ filter contains *dissolved* iron, DFe; the particles trapped on the filter are *particulate* iron, PFe. The average of two samples of marine ice gave 515 nanomolar (nM) DFe and 14,000 nM PFe. These values are much higher than what they found in snow, sea ice, or continental (glacial) ice, where the iron would have come from deposition of atmospheric dust.

The iron in marine ice would be in particles of glacier flour that were suspended in seawater below the ice shelf; the particles would have originated by erosion of bedrock at the base of the ice sheet. HB's Figure 3 shows that many of the particles were clustered in visible bands that were approximately horizontal, as had also been seen in the basal ice of the Ronne Ice Shelf (Figure 10 of Eicken et al., 1994) and in the green iceberg described by Kipfstuhl et al. (1992). The glacier flour would have come from erosion of bedrock in the catchment of the Lambert Glacier and its tributaries (Figure 2). This region contains several rock types, and they do contain substantial iron (Mikhalsky et al., 2001). The Fe_2O_3 content is typically $\sim 2\%$, ranging from 0 to 9% except in the banded ironstone (66%); the FeO content is typically 5%, ranging from 0 to 12%.

In the Amery core, HB reported that the iron concentrations in the marine ice were higher than those in the glacial ice above the transition, by a factor of 5 for DFe and 500 for PFe. To quantify the contribution of this iron to the colors of marine-ice icebergs, we need to consider the chemical form of the iron, and its optical properties. Like DOC, iron-oxide minerals have absorption coefficients that increase with decreasing wavelength from red to blue, so they could likewise shift the color of ice from blue to green.

7. Light Absorption by Iron-Oxide Minerals

The iron in seawater beneath an ice shelf, which can be incorporated into marine ice, will be in small particles containing iron oxides (Cornell & Schwertmann, 1996). Most or all of the iron should be in the ferric state (oxidation state III), because ferrous iron (oxidation state II) rapidly becomes oxidized to ferric iron in water of $\text{pH} > 6$, for any oxygen pressure above a small minimum value, conditions that are well satisfied in seawater (Cornell & Schwertmann, 1996, p. 340). In the surface waters of the Southern Ocean, where oxygen is abundant, 40–60% of the dissolved iron can be Fe (II) (Sarhou et al., 2011), but in those surface waters it is apparently produced by biological reduction, which is unlikely to be active beneath an ice shelf, where sunlight is absent.

Iron in the ferrous state forms soluble compounds, but when oxidized to Fe (III) it precipitates, principally as oxides of varying degrees of hydration. Of course, the precipitated particles may be very small, so as to pass

through a 0.2- μm filter and be classified operationally as $D\text{Fe}$, and hence would be included in our absorption measurements of the dissolved fraction.

Except for hematite, definitive absorption spectra of the ferric oxides at UV and visible wavelengths are scarce, but reflectance spectra are available in many publications. Figure 1 of Scheinost et al. (1998) shows that the positions of the four absorption bands between 400- and 1,000-nm wavelength are similar in seven different forms of ferric oxides: akaganeite, $\beta\text{-FeOOH}$; feroxyhite, $\delta\text{-FeOOH}$; ferrihydrite (also called hydrous ferric oxide), approximately $\text{Fe}(\text{OH})_3$; goethite, $\alpha\text{-FeOOH}$; hematite, $\alpha\text{-Fe}_2\text{O}_3$; lepidocrocite, $\gamma\text{-FeOOH}$; and maghemite, $\gamma\text{-Fe}_2\text{O}_3$.

Reflectance spectra of these minerals across the UV, visible, and near IR, from 0.3 to 2.1 μm , were presented by Sherman et al. (1982) in separate figures. Those spectra were conveniently plotted together in a single figure by Cornell & Schwertmann (1996, Figure 7.5); the seven spectra exhibit considerable similarity. But the magnitude of the reflectance is strongly affected by the particle size and can be similar even for materials whose absorption coefficients differ greatly.

In rocks and soil at the Earth's surface, and in mineral dust in the atmosphere, the iron oxides occur as a mixture with clay minerals and are usually a minor component by mass (2–5%), but they dominate the absorption of visible light. The major iron oxides are hematite and goethite (Schroth et al., 2009; Shi et al., 2012). Goethite is usually more abundant than hematite; Lafon et al. (2006) reported that 25–35% of the iron in dust from the Sahara and Gobi deserts was in the form of hematite, and 65–75% as goethite. For the *reactive* iron available as a micronutrient in the ocean, nanoscale goethite dominates, and it is also the dominant form in marine sediments (van der Zee et al., 2003). Hematite and goethite are close in stability. Hematite can be formed by dehydration of goethite in dry conditions ($2\text{FeOOH} \rightarrow \text{H}_2\text{O} + \text{Fe}_2\text{O}_3$). In water, large particles of hematite are stable, but nanoparticles of hematite (diameter < 100 nm) are metastable relative to goethite (Guo & Barnard, 2013). We therefore expect that the goethite/hematite ratio is higher in the wet conditions of marine-ice formation than in atmospheric aerosol.

Relative absorbance spectra for four of the oxides were shown in Figure 5 of Sherman and Waite (1985). The absorbances of lepidocrocite and maghemite were intermediate between goethite and hematite. We consider hematite and goethite to represent plausible extremes in absorption coefficient for the minerals contributing to the colors of icebergs but recognize that goethite is probably dominant.

7.1. Hematite

Many authors have measured hematite spectra, as reviewed for example by Zhang et al. (2015). There is general agreement about the overall trend: a slow decline from 400 to 550 nm, then a steep decline to 620 nm, then a slow decline again to 800 nm. However, there is not agreement on the actual magnitude of the absorption coefficient; the spread is a factor 3–4 at 400 nm, increasing to a factor of 20 at 700 nm. The most recent measurement is that of Glasscock et al. (2008); their plot approximately traces the median of all reported spectra. Figure 10 compares Glasscock's mass absorption cross section of hematite to that of DOC.

7.2. Goethite

Only two papers have reported an absorption spectrum for goethite, and only one of the two, Bedidi & Cervelle (1993; hereafter BC), has a scale on the graph. However, we think that BC's report should be rejected, as we now explain. BC published spectra of both hematite and goethite, finding goethite a factor of 2–3 less absorptive than hematite. BC started with published measurements of reflectance spectra of these minerals in air and in an oil. From those reflectances, they computed the complex index of refraction $m = m_{re} - i m_{im}$. For hematite, the m_{im} spectrum they obtained (representing absorption) is different from that of all other authors. All other authors show hematite to have a rather steep decline of m_{im} with λ between 550 and 600 nm, but BC show a peak at 580 nm. We therefore do not trust BC's method, so we are inclined to reject BC for both hematite and goethite. Furthermore, when Meland et al. (2011) measured light-scattering patterns from crystals of pure goethite at wavelengths 470, 550, and 660 nm, they were inconsistent with BC's optical constants, substantiating our rejection of BC's values. But Meland et al. were unable to propose revised optical constants for goethite.

The other published absorption spectrum for goethite is that of Sherman & Waite (1985, hereafter SW). SW suspended particles of goethite as a colloidal suspension in water, and measured scattering and attenuation,

inferring absorbance. The spectral shape they found for goethite was similar to that of hematite, but with weaker absorption. (We note that SW's goethite spectrum bears no resemblance to that of BC.) However, SW's absorbance axis lacks a scale, so we cannot get quantitative information for goethite. It may be that the four plots on SW's figure are offset vertically by arbitrary amounts for display, which would account for the lack of a scale.

Even in the absence of a quantitative absorption spectrum for goethite, we might still be able to bound the influence of its iron. Babin and Stramski (2004) showed that the UV-visible absorption of all common minerals was due solely to their iron content. Pure mineral species (quartz, illite, kaolinite, and montmorillonite) had undetectable absorption, but natural mineral assemblages contained some contaminant iron, and their absorption at $\lambda = 400$ nm correlated well with their iron content. When mass-specific absorption B_a was referred to the iron mass rather than to the mineral mass, the values of B_a all were in the restricted range $1\text{--}4$ m²/(g Fe) at $\lambda = 400$ nm. However, this result is challenged by the observation that "a few percent of hematite in a mixture with goethite can mask the yellow goethite colour" (Cornell & Schwertmann, 2003, p. 136), suggesting that the absorption coefficient of goethite is 1–2 orders of magnitude smaller than that of hematite.

8. Color of Ice Containing Iron-Oxide Minerals

To make an accurate computation of the contribution of iron oxides to the colors of icebergs, we would need (a) the iron content of the Amery basal ice, (b) the size distribution of particles in the Amery basal ice, and (c) the mass absorption cross section of goethite as a function of wavelength. For now we have only the iron content. The size distribution of the particles has not yet been measured, and (as explained above) the absorption spectrum of goethite is still unknown. However, we can still make some computations to assess whether the variations of color of marine ice, as seen in icebergs, could plausibly be due to variations in their content of iron oxides.

8.1. Saharan Dust

First, we follow the procedure we have used previously to explain the spectral albedo of snow containing mineral dust (Dang et al., 2015; hereafter DBW). We need the particle size distribution, the density of the mineral, and the real and imaginary parts of its complex index of refraction, $m = m_{re} + im_{im}$. The choices for these quantities were given and justified by DBW, based on numerous measurements of atmospheric dust from deserts, mostly the Sahara. The real index varies slightly with wavelength from 1.50 to 1.55. We take the imaginary index as the solid line in Figure 7 of DBW. We follow DBW in using a lognormal size distribution typical of Asian and Saharan dust, which has mode diameter 0.4 μm , mass-mean diameter 3.5 μm , and effective radius 1.08 μm . The density of the mineral dust material is $2,500$ kg/m³. DBW performed Mie calculations (Wiscombe, 1980) to obtain the single-scattering quantities. Figure 3e of DBW shows the resulting mass absorption cross section, B_a , also plotted here in Figure 10.

Multiplying B_a by the concentration of mineral dust (g/m³) in the ice gives the linear absorption coefficient for dust, k_d (m⁻¹), which can be added to that of ice, k_i . To make use of HB's Fe measurements, we need to convert from concentration of Fe to concentration of dust. We note that in Figure 7 of DBW our $m_{im}(\lambda)$ approximately matches a dust spectrum published by Balkanski et al. (2007) containing 1.5% hematite. Hematite is 70% iron, so Balkanski's dust contained 1.05% Fe. (By comparison, Estapa et al., 2012, estimated 2–5% Fe in riverine and marine sediments.) HB's concentrations of iron are given in nanomolar. Then using the atomic weight of iron, 55.85 daltons, and the density of ice, 917 kg/m³, the conversion from nM Fe to concentration of dust is 4.86 mg \cdot m⁻³ \cdot nM⁻¹. For example, HB's PFe value of 14,000 nM implies that the concentration of dust particles in the iceberg is 68 g/m³. And, for example, at $\lambda = 400$ nm, where $B_a = 0.082$ m²/g, the dust-in-ice absorption coefficient would be $k_d = 5.6$ /m. Combining the absorption coefficients of dust and ice, the absorption spectrum of an iceberg is then $k_a(\lambda) = k_d(\lambda) + k_i(\lambda)$.

Now we ask how much iron is needed to shift the wavelength of minimum absorption from the blue or UV of pure ice to the wavelengths of maximum albedo we measured for green ice and yellow-green ice, 540 and 570 nm, respectively, in Figure 7. Figure 11 shows the results. To shift the color to green requires 700 nM

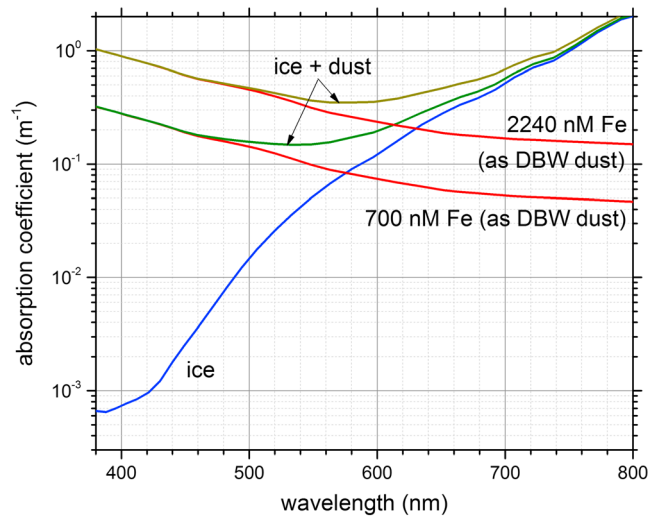


Figure 11. Absorption coefficients of ice and mineral dust, and their sum, for the iron content (700 nM) needed to obtain a wavelength of minimum absorption $\lambda_{\min} = 540$ nm, so as to explain the peak albedo at 540 nm for green marine ice in Figure 7. Also shown is the sum of ice and dust absorption coefficients for an iron content of 2240 nM, needed to obtain $\lambda_{\min} = 570$ nm (yellow-green ice in Figure 7). The optical properties of the dust are from Dang et al. (2015; DBW).

Fe; to yellow-green requires 2240 nM. Recalling that HB found 515 nM of DFe and 14,000 nM of PFe, we can make several comments.

1. The DFe is not quite enough to explain a green color; some of the PFe is also required.
2. The 14,000 nM PFe, with the B_a of atmospheric dust, would shift the color far beyond green, to red, which is not seen in icebergs except in debris-layers.
3. But some aspects of the modeling cause our modeled effect of Fe on color to be exaggerated:
 - a. The optical properties we used are appropriate for desert dust, where hematite is a major contributor to the absorption. (Our conversion between dust concentration and Fe concentration implicitly assumed that the dust consisted of clay minerals containing inclusions of hematite.) In the aqueous environment below an iceberg the hydrated form goethite will instead dominate, and goethite is less absorptive than hematite.
 - b. The average particle size in the marine ice is probably larger than in the atmospheric dust in our calculation. Although the size distribution of particles in the ice was not measured by HB, their Figure 3 does show layers of visible particles that appear to be 20–50 μm in diameter. (In a study of glacier flour produced by erosion under an ice sheet; Hopwood et al., 2014, scanning electron microscopy images of glacier flour show numerous 1- μm particles but a few 10- μm particles which might dominate the mass.) Larger particles have smaller B_a because some of the absorbing material in the interior of the particle is not exposed to light and is therefore wasted. For example, the m_{im} we are using (Figure 7 of DBW) implies an absorption length for the pure dust of 7 μm at $\lambda = 400$ nm, so light entering a particle of diameter 10 μm will be significantly attenuated before reaching the center of the particle.
4. The marine ice in the Amery ice core, in which high concentrations of Fe were found, was not noticeably colored. Similarly, chunks of ice chopped out of blue or green marine-ice icebergs (Figures 3 and 6) also appear colorless. This is because the absorption lengths in ice (reciprocal of the absorption coefficients in Figure 11) are several meters, so that long pathlengths of light through ice are necessary to filter out the more-absorbed wavelengths. The core diameter was only 15 cm, not enough to act as an effective green-filter.

8.2. Montmorillonite

As an alternative to the desert-dust optical properties, we have also tried a less-absorptive mineral, montmorillonite, whose complex refractive index was inferred by Egan and Hilgeman (1979, p. 115) from spectral transmission and reflectance measurements of powder samples with grain size ~ 1 μm . Following Estapa et al. (2012, their Figure 12a), we use the mineral sample from Mississippi, which contains 7.1% Fe by mass. We computed the single-scattering quantities, using the same size distribution we used for the Saharan dust. The mass absorption cross section for montmorillonite is shown in Figure 10; it is weaker than that of Saharan dust by a factor of 1.3. But its iron content is 7 times that of the Saharan dust, so the mass absorption cross section with respect to Fe mass would be about one ninth that of the Saharan dust, smaller than would be expected from the analyses of Babin and Stramski (2004) cited above.

The mixture of montmorillonite in ice results in spectra nearly identical to those of Saharan dust in ice shown in Figure 11, if the Fe concentration is raised by factors of 8–9, as expected. To shift λ_{\min} to 530 nm (green) requires 5600 nM Fe. To obtain $\lambda_{\min} = 570$ nm would require 20,400 nM, which is greater than the sum of DFe + PFe found in the Amery core. The yellow-green ice may have come from a part of the ice shelf that was more heavily loaded with glacial flour than the core samples analyzed by HB, which would also explain the cloudy appearance of the yellow-green ice.

However, we do not claim much significance to this exercise; we have no reason to think montmorillonite from Mississippi is an appropriate representative for the glacier flour under the Amery Ice Shelf. We use

it simply as an illustration for how different minerals can affect the color of the ice. The order-of-magnitude difference in the amount of Fe needed by two different mineral types to shift the color of ice from blue to green motivates further research to measure both iron and DOC in ice whose spectral albedo is also measured.

9. Conclusions, and Recommendations for Further Work

We hypothesize that the iron content found in marine ice, together with the small amount of DOC present, is sufficient to explain the color of green icebergs, and that iron oxides are usually the main contributor to the variation of color within icebergs of marine ice (Figure 7). To confirm or dispute that hypothesis, we recommend taking short cores on icebergs, measuring (a) DOC and POC versus depth, (b) concentrations and size distributions of PFe and DFe, and (c) mineralogy of the iron. In addition, a laboratory measurement of the absorption coefficient of goethite across the visible spectrum is needed, because goethite is most likely the major chemical form of the iron.

A further motivation for such research is that iron is the limiting nutrient for phytoplankton in large areas of the Southern Ocean (Blain et al., 2007; Boyd, 2002; Boyd et al., 2000; de Baar et al., 1990). Research is underway to identify the sources of the iron that does reach the Southern Ocean. The recent finding by Herraiz-Borreguero et al. (2016) that marine ice is rich in iron suggests that icebergs of marine ice can effectively deliver iron to locations far from its origin. If it can be demonstrated that (a) the DOC content of marine ice is routinely too small to significantly affect the reflectance spectrum of icebergs, (b) there is a consistent mineralogy for the iron in the particles, and (c) a consistent size distribution for the particles, then a remote-sensing method might be developed to assay the iron content of icebergs whose marine-ice part is exposed, using reflectance spectroscopy from an instrument deployed on a drone or an airplane.

Acknowledgments

Our albedo measurements and sampling of icebergs in 1988 and 1996 were accomplished on voyages of the Australian National Antarctic Research Expeditions (ANARE); we thank the Australian Antarctic Division for hosting us and for providing excellent logistical support. Petra Heil and Mel Fitzpatrick collected core samples on the icebergs in 1996. The Field Training Officer, Eric Philips, guided us up the icebergs and ensured our safety. Vin Morgan measured the oxygen isotopes on our 1996 icebergs, and Robert Chen measured the DOC. John Gibson provided his DOC analyses of a green iceberg that was sampled at Mawson Station in 1994. Andrea Weiss made some calculations similar to those in Figure 8 as a project for Warren's snow-and-ice class at the University of Washington in 1998. Ben Galton-Fenzi supplied the original for Figure 1. We thank Gerhard Dieckmann and Sepp Kipfstuhl for providing a sample of their green iceberg from 1985 for DOC analysis, and for discussions. We thank Hans Moosmüller, Dariusz Stramski, and Ron Sletten for discussions about the absorption spectra of iron-oxide minerals and Laura Herraiz-Borreguero and Delphine Lannuzel for discussions about their measurements of iron in marine ice. Helpful comments on the manuscript were provided by Martin Vancoppenolle, Ralph Timmermann, and an anonymous reviewer. Our sampling of icebergs in 1996 was supported by NSF grants OPP-95-27244 and OPP-95-27245. Compliance with AGU's Data Policy: All data are given in Table 1 or can be read off the gridded figures.

References

- Amos, A. F. (1978). Green iceberg sampled in the Weddell Sea. *Antarctic Journal of the United States*, 13, 63–64.
- de Baar, H. J., Buma, A., Nolting, R. F., Cadée, G. C., Jacques, G., & Treguer, P. J. (1990). On iron limitation of the Southern Ocean: Experimental observations in the Weddell and Scotia Seas. *Marine Ecology Progress Series*, 65, 105–122. <https://doi.org/10.3354/meps065105>
- Babin, M., & Stramski, D. (2004). Variations in the mass-specific absorption coefficient of mineral particles suspended in water. *Limnology and Oceanography*, 49(3), 756–767. <https://doi.org/10.4319/lo.2004.49.3.0756>
- Balkanski, Y., Schulz, M., Claquin, T., & Guibert, S. (2007). Reevaluation of mineral aerosol radiative forcings suggests a better agreement with satellite and AERONET data. *Atmospheric Chemistry and Physics*, 7(1), 81–95. <https://doi.org/10.5194/acp-7-81-2007>
- Bedidi, A., & Cervelle, B. (1993). Light scattering by spherical particles with hematite and goethite-like optical properties: Effect of water impregnation. *Journal of Geophysical Research*, 98(B7), 11,941–11,952. <https://doi.org/10.1029/93JB00188>
- Binder, A. R. (1972). Black and white icebergs, Southern Ocean. *Marine Observer*, 42, 15–16.
- Blain, S., Quéguiner, B., Armand, L., Belviso, S., Bombled, B., Bopp, L., Bowie, A., et al. (2007). Effect of natural iron fertilization on carbon sequestration in the Southern Ocean. *Nature*, 446(7139), 1070–1074. <https://doi.org/10.1038/nature05700>
- Boyd, P. W. (2002). Environmental factors controlling phytoplankton processes in the Southern Ocean. *Journal of Phycology*, 38(5), 844–861. <https://doi.org/10.1046/j.1529-8817.2002.t01-1-01203.x>
- Boyd, P. W., Watson, A. J., Law, C. S., Abraham, E. R., Trull, T., Murdoch, R., et al. (2000). A mesoscale phytoplankton bloom in the polar Southern Ocean stimulated by iron fertilization. *Nature*, 407(6805), 695–702. <https://doi.org/10.1038/35037500>
- Bricaud, A., Morel, A., & Prieur, L. (1981). Absorption by dissolved organic matter of the sea (yellow substance) in the UV and visible domains. *Limnology and Oceanography*, 26(1), 43–53. <https://doi.org/10.4319/lo.1981.26.1.0043>
- Cornell, R. M., & Schwertmann, U. (1996). *The iron oxides*, (p. 573). Weinheim, Germany: VCH Publisher.
- Cornell, R. M., & Schwertmann, U. (2003). *The iron oxides*, (2nd ed., p. 694). Weinheim, Germany: VCH Publisher. <https://doi.org/10.1002/3527602097>
- Curran, M. A. J., & Palmer, S. S. (2001). Suppressed ion chromatography methods for the routine determination of ultra low level anions and cations in ice cores. *Journal of Chromatography A*, 919(1), 107–113. [https://doi.org/10.1016/S0021-9673\(01\)00790-7](https://doi.org/10.1016/S0021-9673(01)00790-7)
- Dang, C., Brandt, R. E., & Warren, S. G. (2015). Parameterizations for narrowband and broadband albedo of pure snow, and snow containing mineral dust and black carbon. *Journal of Geophysical Research: Atmospheres*, 120, 5446–5468. <https://doi.org/10.1002/2014JD022646>
- van der Zee, C., Roberts, D. R., Rancours, D. G., & Slomp, C. P. (2003). Nanogoethite is the dominant reactive oxyhydroxide phase in lake and marine sediments. *Geology*, 31, 993–996.
- Dieckmann, G., Hemleben, C., & Spindler, M. (1987). Biogenic and mineral inclusions in a green iceberg from the Weddell Sea, Antarctica. *Polar Biology*, 7(1), 31–33. <https://doi.org/10.1007/BF00286821>
- Drygalski, E. V. (1921). Deutsche Südpolar-Expedition, 1901–1903, vol. 1, part 3, p. 547, Vereinigung Wissenschaftlicher Verleger, Berlin & Leipzig.
- Dutrieux, P., Stewart, C., Jenkins, A., Nicholls, K. W., Corr, H. F. J., Rignot, E., & Steffen, K. (2014). Basal terraces on melting ice shelves. *Geophysical Research Letters*, 41, 5506–5513. <https://doi.org/10.1002/2014GL060618>
- Egan, W. G., & Hilgeman, T. W. (1979). *Optical properties of inhomogeneous materials*, (p. 235). New York: Academic Press.
- Eicken, H., Oerter, H., Miller, H., Graf, W., & Kipfstuhl, J. (1994). Textural characteristics and impurity content of meteoric and marine ice in the Ronne Ice Shelf, Antarctica. *Journal of Glaciology*, 40(135), 386–398. <https://doi.org/10.1017/S0022143000007474>

- Estapa, M. L., Boss, E., Mayer, L. M., & Roesler, C. S. (2012). Role of iron and organic carbon in mass-specific light absorption by particulate matter from Louisiana coastal waters. *Limnology and Oceanography*, *57*(1), 97–112. <https://doi.org/10.4319/lo.2012.57.1.0097>
- Fichot, C. G., & Benner, R. (2011). A novel method to estimate DOC from CDOM absorption coefficients in coastal waters. *Geophysical Research Letters*, *38*, L03610. <https://doi.org/10.1029/2010GL046152>
- Fricker, H. A., Popov, S., Allison, I., & Young, N. (2001). Distribution of marine ice beneath the Amery Ice Shelf. *Geophysical Research Letters*, *28*(11), 2241–2244. <https://doi.org/10.1029/2000GL012461>
- Galton-Fenzi, B. K., Hunter, J. R., Coleman, R., Marsland, S. J., & Warner, R. C. (2012). Modeling the basal melting and marine ice accretion of the Amery Ice Shelf. *Journal of Geophysical Research*, *117*, C09031. <https://doi.org/10.1029/2012JC008214>
- Glasscock, J. A., Barnes, P. R. F., Plumb, I. C., Bendavid, A., & Martin, P. J. (2008). Structural, optical and electrical properties of undoped polycrystalline hematite thin films produced using filtered arc deposition. *Thin Solid Films*, *516*(8), 1716–1724. <https://doi.org/10.1016/j.tsf.2007.05.020>
- Guo, H., & Barnard, A. S. (2013). Naturally occurring iron oxide nanoparticles: Morphology, surface chemistry and environmental stability. *Journal of Materials Chemistry*, *1*(1), 27–42. <https://doi.org/10.1039/C2TA00523A>
- Hansell, D. A., & Carlson, C. A. (1998). Deep-ocean gradients in the concentration of dissolved organic carbon. *Nature*, *395*(6699), 263–266. <https://doi.org/10.1038/26200>
- Hansen, A. M., Kraus, T. E. C., Pellerin, B. A., Fleck, J. A., Downing, B. D., & Bergamaschi, B. A. (2016). Optical properties of dissolved organic matter (DOM): Effects of biological and photolytic degradation. *Limnology and Oceanography*, *61*(3), 1015–1032. <https://doi.org/10.1002/lno.10270>
- Herraiz-Borreguero, L., Lannuzel, D., van der Merwe, P., Treverrow, A., & Pedro, J. B. (2016). Large flux of iron from the Amery Ice Shelf marine ice to Prydz Bay, East Antarctica. *Journal of Geophysical Research: Oceans*, *121*, 6009–6020. <https://doi.org/10.1002/2016JC011687>
- Hoffman, P. F., Abbot, D. S., Ashkenazy, Y., Benn, D. I., Cohen, P. A., Cox, G. M., et al. (2017). Climate dynamics of Snowball Earth and Cryogenian geology-geobiology. *Science Advances*, *3*, e1600983. <https://doi.org/10.1126/sciadv.1600983>
- Hopwood, M. J., Statham, P. J., Tranter, M., & Wadham, J. L. (2014). Glacial flours as a potential source of Fe (II) and Fe (III) to polar waters. *Biogeochemistry*, *118*(1-3), 443–452. <https://doi.org/10.1007/s10533-013-9945-y>
- Jerlov, N. G. (1968). *Optical Oceanography*. New York: Elsevier Pub.
- Khazendar, A., Tison, J. L., Stenni, B., Dini, M., & Bondesan, A. (2001). Significant marine-ice accumulation in the ablation zone beneath an Antarctic ice shelf. *Journal of Glaciology*, *47*(158), 359–368. <https://doi.org/10.3189/172756501781832160>
- Kipfstuhl, J., Dieckmann, G., Oerter, H., Hellmer, H., & Graf, W. (1992). The origin of green icebergs in Antarctica. *Journal of Geophysical Research*, *97*(C12), 20,319–20,324. <https://doi.org/10.1029/92JC01754>
- Kovacs, A. (1996). Sea ice, Part I: Bulk salinity versus ice floe thickness, CRREL Report 96-7, U.S. Army Cold Regions Research and Engineering Laboratory, Hanover, NH, USA, 17 pp.
- Lafon, S., Sokolik, I. N., Rajot, J. L., Caquineau, S., & Gaudichet, A. (2006). Characterization of iron oxides in mineral dust aerosols: Implications for light absorption. *Journal of Geophysical Research*, *111*, D21207. <https://doi.org/10.1029/2005JD007016>
- Light, B., Maykut, G. A., & Grenfell, T. C. (2003). Effects of temperature on the microstructure of first-year Arctic sea ice. *Journal of Geophysical Research*, *108*(C2), 3051. <https://doi.org/10.1029/2001JC000887>
- Meland, B., Kleiber, P., Grassian, V., & Young, M. (2011). Visible light scattering study at 470, 550, and 660 nm of components of mineral dust aerosol: Hematite and goethite. *Journal of Quantitative Spectroscopy and Radiative Transfer*, *112*(6), 1108–1118. <https://doi.org/10.1016/j.jqsrt.2010.12.002>
- Mikhalsky, E. V., Sheraton, J. W., Laiba, A. A., Tingey, R. J., Thost, D. E., Kamenev, E. N., & Fedorov, L. V. (2001). Geology of the Prince Charles Mountains, Antarctica, AGSO Geoscience Australia Bulletin 247, Pub. Geoscience Australia, 211 pp.
- Moreau, S., Vancoppenolle, M., Zhou, J., Tison, J.-L., Delille, B., & Goosse, H. (2014). Modelling argon dynamics in first-year sea ice. *Ocean Modelling*, *73*, 1–18. <https://doi.org/10.1016/j.ocemod.2013.10.004>
- Morel, A., & Prieur, L. (1977). Analysis of variations in ocean color. *Limnology and Oceanography*, *22*(4), 709–722. <https://doi.org/10.4319/lo.1977.22.4.0709>
- Morgan, V. I. (1972). Oxygen isotope evidence for bottom freezing on the Amery Ice Shelf. *Nature*, *238*(5364), 393–394. <https://doi.org/10.1038/238393a0>
- Moulton, K. N., & Cameron, R. L. (1976). Bottle-green iceberg near the South Shetland Islands. *Antarctic Journal of the United States*, *11*, 94–95.
- Nelson, N. B., & Siegel, D. A. (2013). The global distribution and dynamics of chromophoric dissolved organic matter. *Annual Review of Marine Science*, *5*(1), 447–476. <https://doi.org/10.1146/annurev-marine-120710-100751>
- Oerter, H., Kipfstuhl, J., Determann, J., Miller, H., Wagenbach, D., Minikin, A., & Graf, W. (1992). Evidence for basal marine ice in the Filchner-Ronne ice shelf. *Nature*, *358*(6385), 399–401. <https://doi.org/10.1038/358399a0>
- Ogawa, H., Fukuda, R., & Koike, I. (1999). Vertical distributions of dissolved organic carbon and nitrogen in the Southern Ocean. *Deep Sea Research Part I: Oceanographic Research Papers*, *46*(10), 1809–1826. [https://doi.org/10.1016/S0967-0637\(99\)00027-8](https://doi.org/10.1016/S0967-0637(99)00027-8)
- Peltzer, E. T., & Hayward, N. A. (1996). Spatial and temporal variability of total organic carbon along 140°W in the equatorial Pacific Ocean in 1992. *Deep-Sea Research Part II: Topical Studies in Oceanography*, *43*, 1155–1180.
- Perovich, D. K., Cota, G. F., Maykut, G. A., & Grenfell, T. C. (1993). Bio-optical observations of first-year Arctic sea ice. *Geophysical Research Letters*, *20*(11), 1059–1062. <https://doi.org/10.1029/93GL01316>
- Reichelt, W. (1941). Die ozeanographischen Verhältnisse bis zur warmen Zwischenschicht an der antarktischen Eisgrenze im Südsommer 1936/37. *Archiv der Deutschen Seewarte und des Marineobservatoriums*, *61*(5), 55.
- Roesler, C. S., & Iturriaga, R. H. (1994). Absorption properties of marine-derived material in Arctic sea ice, Paper presented at Ocean Optics XII, International Society for Optics and Photonics.
- Russell, P. B., Bergstrom, R. W., Shinozuka, Y., Clarke, A. D., DeCarlo, P. F., Jimenez, J. L., et al. (2010). Absorption Angstrom Exponent in AERONET and related data as an indicator of aerosol composition. *Atmospheric Chemistry and Physics*, *10*(3), 1155–1169. <https://doi.org/10.5194/acp-10-1155-2010>
- Sarthou, G., Bucciarelli, E., Chever, F., Hansard, S. P., Gonzalez-Davila, M., Santana-Casiano, J. M., et al. (2011). Labile Fe (II) concentrations in the Atlantic sector of the Southern Ocean along a transect from the subtropical domain to the Weddell Sea Gyre. *Biogeochemistry*, *8*(9), 2461–2479. <https://doi.org/10.5194/bg-8-2461-2011>
- Scheinost, A. C., Chavernas, A., Barron, V., & Torrent, J. (1998). Use and limitations of second-derivative diffuse reflectance spectroscopy in the visible to near-infrared range to identify and quantify Fe oxide minerals in soils. *Clays and Clay Minerals*, *46*(5), 528–536. <https://doi.org/10.1346/CCMN.1998.0460506>

- Schroth, A. W., Crusius, J., Sholkovitz, E. R., & Bostick, B. C. (2009). Iron solubility driven by speciation in dust sources to the ocean. *Nature Geoscience*, 2(5), 337–340. <https://doi.org/10.1038/ngeo501>
- Sherman, D. M., Burns, R. G., & Burns, V. M. (1982). Spectral characteristics of the iron oxides with application to the Martian bright region mineralogy. *Journal of Geophysical Research*, 87(B12), 10,169–10,180. <https://doi.org/10.1029/JB087iB12p10169>
- Sherman, D. M., & Waite, T. D. (1985). Electronic spectra of Fe³⁺ oxides and oxide hydroxides in the near IR to near UV. *American Mineralogist*, 70, 1262–1269.
- Shi, Z., Krom, M. D., Jickells, T. D., Bonneville, S., Carslaw, K. S., Mihalopoulos, N., et al. (2012). Impacts on iron solubility in the mineral dust by processes in the source region and the atmosphere: A review. *Aeolian Research*, 5, 21–42. <https://doi.org/10.1016/j.aeolia.2012.03.001>
- Silvano, A., Rintoul, S. R., & Herraiz-Borreguero, L. (2016). Ocean-ice shelf interaction in East Antarctica. *Oceanography*, 29, 131–143.
- Tabraham, J. (1997). The desalination of marine ice, Ph.D. Dissertation, University of Cambridge, 177 pp.
- Tsurikov, V. L. (1979). The formation and composition of the gas content of sea ice. *Journal of Glaciology*, 22(86), 67–81. <https://doi.org/10.1017/S0022143000014064>
- Twardowski, M. S., Boss, E., Sullivan, J. M., & Donaghay, L. (2004). Modeling the spectral shape of absorption by chromophoric dissolved organic matter. *Marine Chemistry*, 89(1-4), 69–88. <https://doi.org/10.1016/j.marchem.2004.02.008>
- Vlahos, P., Chen, R. F., & Repeta, D. J. (2002). Fluxes of dissolved organic carbon (DOC) in the Mid-Atlantic Bight. *Deep-Sea Research*, 49(20), 4369–4385. [https://doi.org/10.1016/S0967-0645\(02\)00167-4](https://doi.org/10.1016/S0967-0645(02)00167-4)
- Wadhams, P. (2000). Ice in the ocean. Gordon and Breach Pub., 351 pp.
- Warren, S. G., & Brandt, R. E. (2008). Optical constants of ice from the ultraviolet to the microwave: A revised compilation. *Journal of Geophysical Research*, 113, D14220. <https://doi.org/10.1029/2007JD009744>
- Warren, S. G., Roesler, C. S., & Brandt, R. E. (1997). Solar radiation processes in the East Antarctic sea ice zone. *Antarctic Journal of the United States*, 32, 185–187.
- Warren, S. G., Roesler, C. S., Morgan, V. I., Brandt, R. E., Goodwin, I. D., & Allison, I. (1993). Green icebergs formed by freezing of organic-rich seawater to the base of Antarctic ice shelves. *Journal of Geophysical Research*, 98(C4), 6921–6928. <https://doi.org/10.1029/92JC02751>
- Wiscombe, W. J. (1980). Improved Mie scattering algorithms. *Applied Optics*, 19(9), 1505–1509. <https://doi.org/10.1364/AO.19.001505>
- Wordie, J. M., & Kemp, S. (1933). Observations on certain Antarctic icebergs. *The Geographical Journal*, 81(5), 428–434. <https://doi.org/10.2307/1786610>
- Yacobi, Y. Z., Alberts, J. J., Takacs, M., & McElvaine, M. (2003). Absorption spectroscopy of colored dissolved organic carbon in Georgia (USA) rivers: The impact of molecular size distribution. *Journal of Limnology*, 62(1), 41–46. <https://doi.org/10.4081/jlimnol.2003.41>
- Zhang, X. L., Wu, G. J., Zhang, C. L., Xu, T. L., & Zhou, Q. Q. (2015). What is the real role of iron oxides in the optical properties of dust aerosols? *Atmospheric Chemistry and Physics*, 15(21), 12,159–12,177. <https://doi.org/10.5194/acp-15-12159-2015>